SCIREA Journal of Materials

http://www.scirea.org/journal/Materials

June 8, 2021

Volume 6, Issue 3, June 2021

Anti-oxidation mechanism investigation of SiO_2+SiC+Al $(H_2PO_4)_3$ coating for continuous SiC fiber reinforced $AlPO_4$ composites with multi-walled carbon nanotubes as the absorber

Xi Xia[a,b], Feng Wan[a,b,*], Jianhui Yan[a,b], Hongmei Xu[a,b], KaiDi Hu[a,b]

[a] School of Materials Science and Engineering, Hunan University of Science and Technology, Xiangtan, Hunan 411201, China

[b] Hunan Provincial Key Laboratory of Advanced Materials for New Energy Storage and Conversion, Hunan University of Science and Technology, Xiangtan, Hunan 411201, China

* Corresponding author. Tel:+ 86 073158290732; fax: +86 073158290732

Email address: wanfenghkd@163.com (F- Wan)

Abstract

$SiC_f/AlPO_4$ composites were fabricated using a hot laminating process with MWCNTs as the absorber. A coating prepared from SiO_2+SiC+Al $(H_2PO_4)_3$ was applied to the surface of $SiC_f/AlPO_4$ composites prior to an anti-oxidation test at 1373 K in air for 40 h. The anti-oxidation effect was verified by a three-point bending test, scanning electron microscopy, transmission electron microscopy, X-ray diffraction and a dielectric property test. Anti-oxidation mechanism investigations revealed that the coating effectiveness could be

attributed to three substances, i.e. SiO_2, SiP_2O_7 and SiO_2 +$AlPO_4$ solid solution from the reactions of $SiC+O_2 \rightarrow SiO_2+CO$, $SiO_2+P_2O_5 \rightarrow SiP_2O_7$ and SiO_2 +$AlPO_4 \rightarrow$ solid solution, respectively.

Keywords: SiC fibers; Oxidation; SiP_2O_7; Solid solution

Introduction

Electromagnetic wave absorbing materials, designed to decrease reflected electromagnetic radiation by absorbing electromagnetic waves and transforming it into other energy, is a topic of extensive interest in the aerospace and military fields [1-8]. Currently, the research for applications in high-temperature environments is the main topic for electromagnetic wave absorbing materials.

Various ceramic matrix composites, showing excellent fracture toughness, good thermal stability and environmental durability have been evaluated and modified for use as structural electromagnetic wave absorbing materials [9-15]. Among this, continuous SiC fiber reinforced $AlPO_4$ ($SiC_f/AlPO_4$) composites have demonstrated good potential. Their excellent mechanical properties, low dielectric constants provide the opportunity to tailor the dielectric properties and wave absorbing abilities by the addition of conductive fillers [16, 17]. At the same time, the deterioration of SiC fibers (phase transformation and grain growth) in $SiC_f/AlPO_4$ composites during fabrication process can be controlled. The desirable mechanical properties of the composites are not compromised at the low temperatures used during curing [18, 19], compared to the high temperature sintering processes used to prepare Al_2O_3 and $3Al_2O_3 \cdot 2SiO_2$ ceramics [20].

The long-term and stable electromagnetic wave absorbing performance of $SiC_f/AlPO_4$ composites is highly dependent on the incorporated absorber. In an oxidizing atmosphere, an effective coating is required to prevent the absorber from being consumed. Currently, few studies concerning the preparation of anti-oxidation coatings for $SiC_f/AlPO_4$ composites have

been published.

In this study, the $SiC_f/AlPO_4$ composites were prepared by lamination with multi-walled carbon nanotubes (MWCNTs) for fine tuning of the dielectric property. A coating, derived from SiO_2+SiC+Al $(H_2PO_4)_3$ was prepared and coated $SiC_f/AlPO_4$ composites were subjected to an anti-oxidation test at 1373 K in air for 40 h. The anti-oxidation efficiency of the coating was proved and examined in detail.

SiC fibers were provided by the National University of Defense Technology (China). Figure. 1(a) and Figure. 1(b) show the SEM image of 50 vol. % 2D SiC cloth and TEM image of MWCNTs, respectively. The diameter of SiO_2 and β-SiC powders were in the range of 1-5 μm. $SiC_f/AlPO_4$ composites were prepared according to Ref. [16].

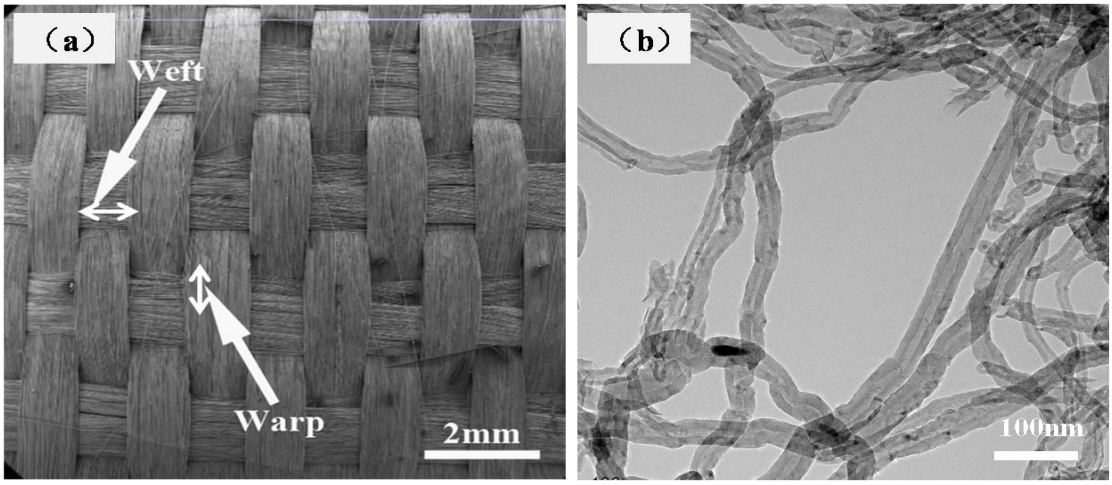

Fig. 1. (a) 2D SiC fibers cloth and (b) TEM image of MWCNTs.

$Al(H_2PO_4)_3$ solution was mixed with the SiO_2 and SiC powders in the ratio 5:3:2 (w/w) $Al(H_2PO_4)_3$: SiO_2: SiC. After ball milling for 3 h, the obtained mixture was brushed onto the surface of $SiC_f/AlPO_4$ composites and dried at 373 K for 1 h prior to annealing at 1473 K for 3 h at a heating rate of 283 K/min in vacuum atmosphere. After cooling at ambient temperature, the sample was given two infiltration-drying-annealing cycles to yield the coated $SiC_f/AlPO_4$ composites. Uncoated and coated $SiC_f/AlPO_4$ composites were heated to 1373 K (40 h hold) in a muffle furnace. Treated samples were cooled to room temperature under ambient conditions.

Morphology and microstructure were characterized by SEM (ZEISS Supra 55, Germany) and

TEM (G-20, FEI-Tecnai, USA). Phase evolution characterizations were determined by X-ray diffraction (XRD; X'Pert Pro, Philips, Netherlands). The bending strength (σ) of $SiC_f/AlPO_4$ composites at room temperature was obtained by a three-point bending test, following the general guidelines of ASTM standard C1341. The complex permittivity values for $SiC/AlPO_4$ composites were determined from the measurements of the reflection and transmission module between 8.2GHz and 12.4 GHz [21, 22].

The bending strength for $SiC_f/AlPO_4$ composites obtained by the three-point bending test are reflected in Fig. 2(a). The three specimens initially showed an elastic response with increasing displacement. After reaching the maximum strength, the bending strength of the as-received specimen displayed an inelastic decrease before reducing abruptly. This differed from the curves of the oxidized specimens (with and without the coating) which showed a direct reduction in bending strength at maximum strength. The brittle fracture for the three curves could be attributed to the absence of an interface, loss of toughening mechanisms due to fiber pull-out and debonding, and crack deflection. After oxidizing for 40 h, the bending strength of the coated specimen decreased from 205 MPa to 190 MPa and the displacement was reduced to 0.38 mm. These effects were due to the influence of high temperature on the SiC fibers. The specimen without the coating attained a bending strength 60 MPa and displacement of 0.14 mm. The corresponding fracture surface morphologies of the specimens (with and without the coating) subjected to oxidizing conditions are given in Fig. 2(b) and Fig. 2(c), respectively. The fracture surface of the coated specimen was smooth and little fiber pull-out was observed (Fig. 2(b)). The cross sections of SiC fibers were complete and clearly visible. Figure. 2(c) shows the SEM and TEM pictures of uncoated $SiC_f/AlPO_4$ composites undergoing 40h oxidation. Obviously, a strong bond occurred and a reaction zone was formed between $AlPO_4$ matrix and SiC fiber, which could be attributed to the reaction of $AlPO_4$ matrix and SiO_2, produced from the oxidation of SiC (see also section 3.2).

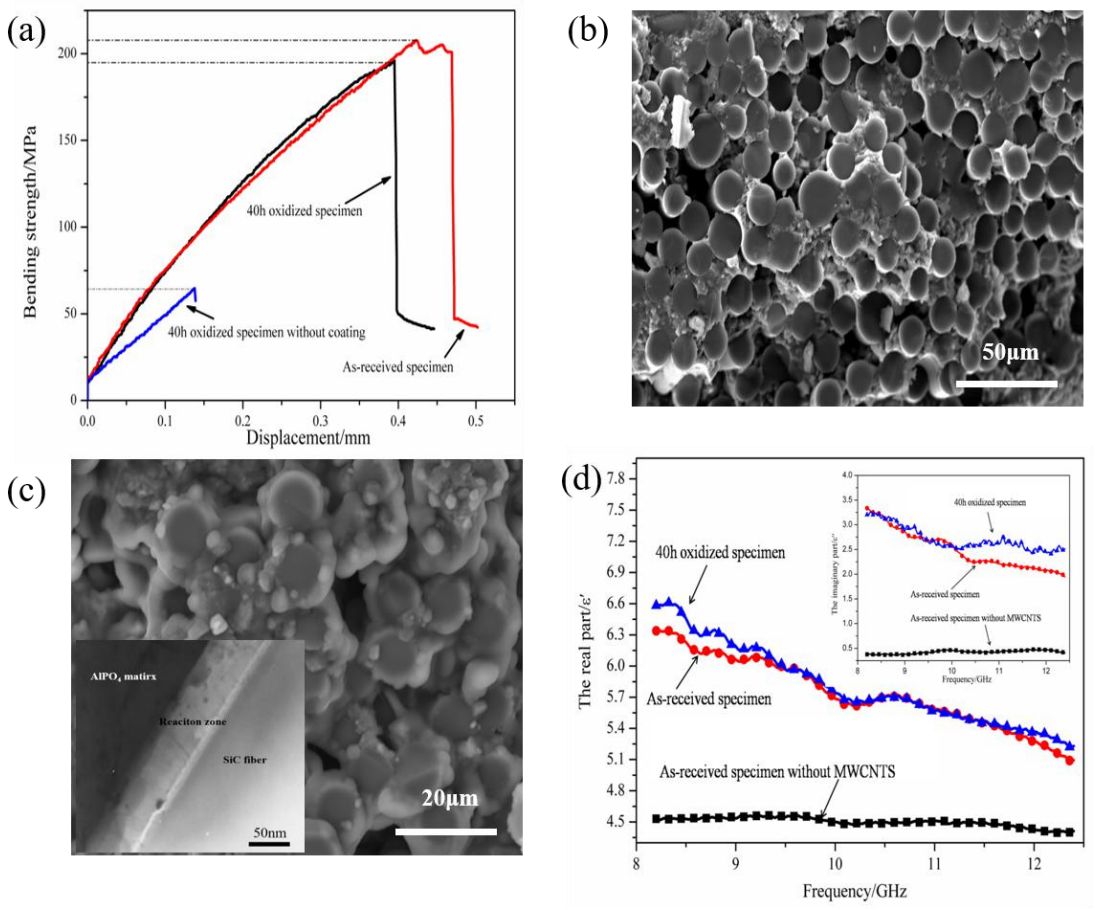

Fig. 2. (a) Typical stress-displacement curves of $SiC_f/AlPO_4$ composites, (b) SEM image of coated $SiC_f/AlPO_4$ composites after oxidization, (c) SEM and TEM images of uncoated $SiC_f/AlPO_4$ composites after oxidization and (d) complex permittivity of $SiC_f/AlPO_4$ composites.

The real part (ε') and imaginary part (ε″) of the complex permittivity for the $SiC_f/AlPO_4$ composites are shown in the dielectric permittivity spectrum of Fig. 2(d), which were closely correlated with the MWCNTs. When no MWCNTs are added, the ε' and ε″ values for the coated $SiC_f/AlPO_4$ composites were in the range of 4.2-4.5 and 0.2-0.5 within the entire X-band, respectively. With the introduction of 1.5 wt. % MWCNTs, the ε' and ε″ ranges increased from 4.2-4.5 to 5.0-6.3 and 0.2-0.5 to 1.8-3.6 respectively. After oxidation, the values of ε' and ε″ for the coated $SiC_f/AlPO_4$ composites with 1.5wt.% MWCNTs showed little change compared with the values before oxidation. These results showed that the MWCNTs were still present and functional.These findings demonstrated that the anti-oxidation effect of the coating was effective for the $SiC_f/AlPO_4$ composites in an oxidizing environment at 1373 K.

Fig. 3(a) shows the SEM image of coated $SiC_f/AlPO_4$ composites before oxidization. The coating formed a strong bond with the $AlPO_4$ matrix, and no obvious boundary was distinguished (indicated by the black arrows). In addition, the particles in coating were dispersed evenly and chemically bonded. According to the phase diagram of $AlPO_4$-SiO_2 [23], some phases of solid solution (C- $AlPO_4$ solid solution, T- $AlPO_4$ solid solution, Cr- SiO_2 solid solution, Tr- SiO_2 solid solution) might be formed when the preparation temperature of the coating was maintained at 1473K, and these were dependent on the content of $AlPO_4$ and SiO_2 in mixture. Consequently, this result was theoretically responsible for the strong bond between the $AlPO_4$ matrix and the coating. The XRD spectrum of reaction products derived from $Al(H_2PO_4)_3$ solution and SiO_2 is reflected in Fig. 3(b). Four major peaks around 2θ values of 20.4°，24.2°，25.9° and 30.4° (at 10 wt. % SiO_2), were homologous with the crystal phase of $Al(PO_3)_3$ and decreased in intensity with the increasing content of SiO_2 and were absent at 40 wt.% SiO_2. However, the intensity of the two peaks around 2θ values of 20.8° and 26.5° increased. Supposing these peaks were ensured to be SiO_2, the disappearance of $Al(PO_3)_3$ peaks could not be accepted; if they are ensured to be $AlPO_4$ (i.e. decomposition products of $Al(PO_3)_3$), the disappearance of SiO_2 peaks could not be accepted. Hence, it was concluded that the SiO_2 reacted with $AlPO_4$ to form solid solution, which was responsible for the diffraction peaks in XRD spectrum of 40 wt.% SiO_2. The continuous decomposition and final exhaustion for $Al(PO_3)_3$ was attributed to the consumption of $AlPO_4$ from an abundance of SiO_2. Hence the results given in Fig. 2(c) and Fig. 3(b) experimentally confirm that the SiO_2 -$AlPO_4$ solid solution was tightly correlated with the strong bond between the $AlPO_4$ matrix and the coating.

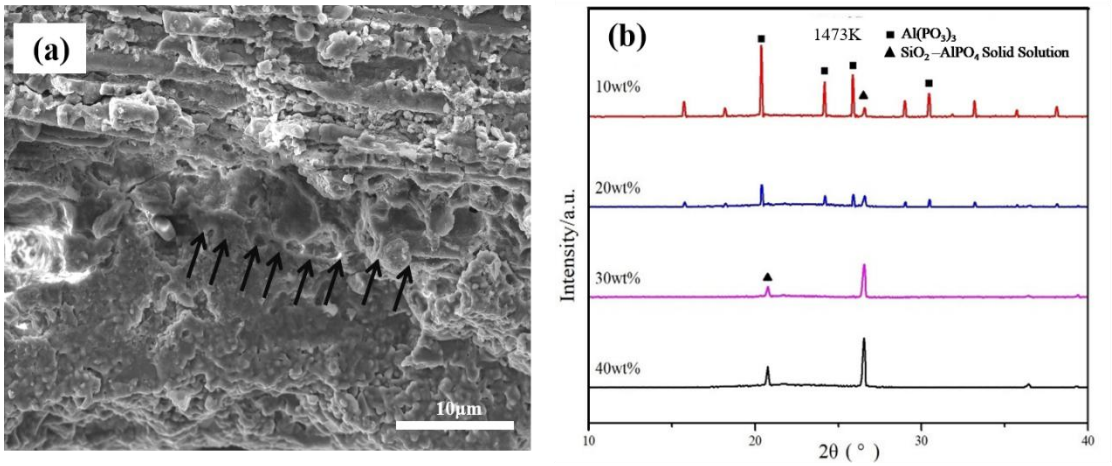

Fig. 3. (a) Cross section SEM image of coated $SiC_f/AlPO_4$ composite and (b) XRD spectrum of products derived from the reaction between Al $(H_2PO_4)_3$ and SiO_2.

The presence of low melting point SiP_2O_7, derived from the reaction of SiO_2 and P_2O_5 ($Al(PO_3)_3 \rightarrow AlPO_4 + P_2O_5$), also strengthened the bonding within the coating. This could be confirmed by the phase diagram of SiO_2-P_2O_5 [24]. These two chemical reactions contributed to the formation of a dense coating.

The SEM image of coated $SiC_f/AlPO_4$ composites following heating at 1373 K for 40 h can be seen in Fig. 4(a): More glassy substances (SiP_2O_7) were observed in this sample compared with the specimen that had not been subjected to the oxidizing conditions (see Fig. 3(a)). During the preparation of the coating, P_2O_5 (g) is readily released while and the formation of SiP_2O_7 slows. However, the relatively long oxidation time was enough for P_2O_5 to react with SiO_2 and form SiP_2O_7.

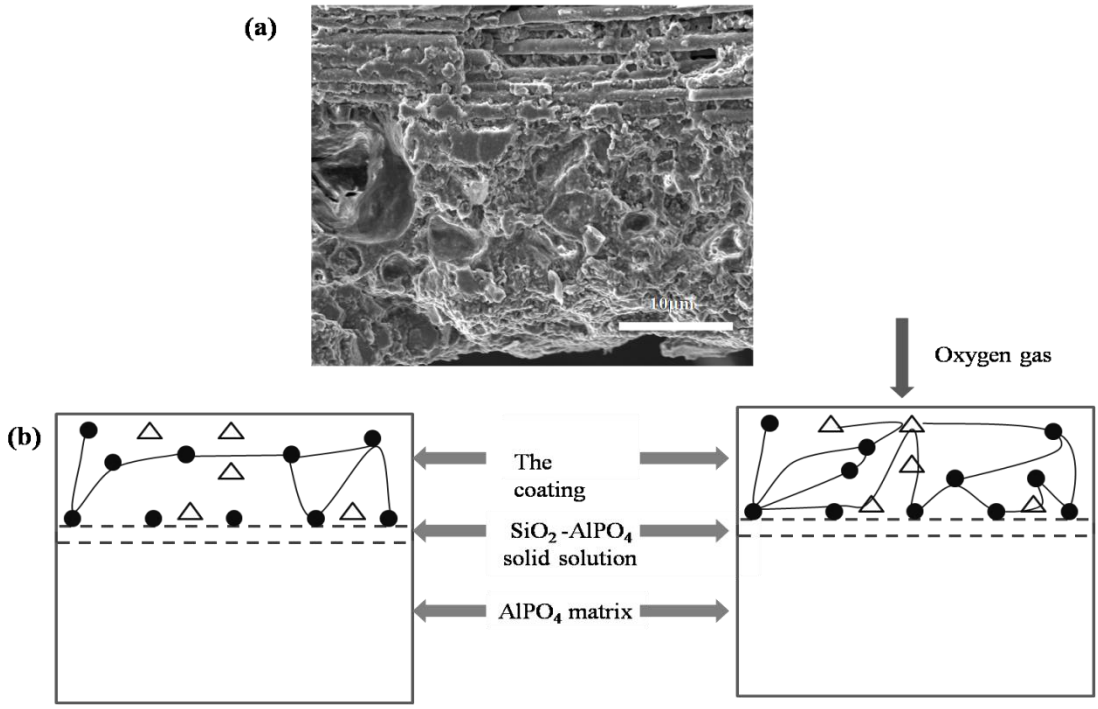

Fig. 4. (a) Cross section SEM image of coated $SiC_f/AlPO_4$ composite after oxidization and (b) schematic diagram of anti-oxidation mechanism for the coating.

Table. 1 shows the calculated Gibbs free energy (ΔG) for the oxidation of SiC at 1373 K: The reaction shown by Eq. (4) was favored by its minimal value of ΔG. As oxygen gas is introduced, SiC particles are oxidized to SiO_2 which then reacts with P_2O_5 and $AlPO_4$. The integration of SiO_2, SiP_2O_7 and SiO_2 -$AlPO_4$ solid solution into the coating is effective in preventing the oxygen gas from further diffusion into the $SiC_f/AlPO_4$ composite.

Table 1 The ΔG of SiC oxidation.

Code	Reaction	ΔG/KJ/mol at 1373K
(1)	$SiC+1/2O_2 \Leftrightarrow SiO(g)+C$	-156.07
(2)	$SiC+O_2 \Leftrightarrow SiO_2+C$	-632.91
(3)	$SiC+O_2 \Leftrightarrow SiO(g)+CO(g)$	-379.94
(4)	$SiC+3/2O_2 \Leftrightarrow SiO_2+CO(g)$	-855.27
(5)	$C+1/2O_2 \Leftrightarrow CO(g)$	-223.59

Fig. 4(b) gives a summary schematic representation of the mechanism of anti-oxidation based on the results from this study. During preparation of the coating, the $AlPO_4$ matrix reacts with SiO_2 to from a SiO_2 -$AlPO_4$ solid solution leading to a strong chemical bond between $SiC_f/AlPO_4$ composite and the coating. The formation of SiP_2O_7 and SiO_2 -$AlPO_4$ solid

solution facilitates the bonding of the particles in coating which contributes to the formation of a dense coating. Under oxidizing conditions, the SiC in the coating is partially transformed into SiO_2 as it consumes the incoming oxygen gas and the decomposition of $Al(PO_3)_3$ increases with the increasing time. The reactions of SiO_2 -$AlPO_4$ and SiO_2 -P_2O_5 occur throughout the coating, linking particles to form a dense coating of low oxygen permeability.

In summary, this study presents a detailed investigation of anti-oxidation mechanism of the SiO_2+SiC+$Al(H_2PO_4)_3$ coating. The anti-oxidation effect of the $SiC_f/AlPO_4$ composites in oxidizing environment (1373 K, 40 h) were confirmed by a three-point bending test, microstructure characterization and dielectric property. $SiC_f/AlPO_4$ composites were chemically bonded with the coating. Oxygen gas in the environment was consumed by SiC particles to form SiO_2 which subsequently reacted with P_2O_5 and $AlPO_4$ to form SiP_2O_7 and SiO_2 -$AlPO_4$ solid solution, respectively. The integration of SiO_2, SiP_2O_7 and SiO_2 -$AlPO_4$ solid solution into the coating was effective in preventing the oxygen gas from consuming MWCNTs. The coating gives $SiC_f/AlPO_4$ composites the potential to be applied as high-temperature structural wave absorbing materials.

Acknowledgements

This work is jointly supported by National Natural Science Foundation of China (Grant No. 51802095), the Natural Science Foundation of Hunan Province (Grant No. 2019JJ50165).

References:

[1] H. Wang, D. Zhu, X. Wang, F. Luo, Composites Part A: Applied Science and Manufacturing, 93 (2017) 10-17.

[2] Q. Zhang, Y. Gou, J. Wang, H. Wang, K. Jian, Y. Wang, Journal of the European Ceramic Society, 37 (2017) 1909-1916.

[3] T. Shao, H. Ma, J. Wang, M. Feng, M. Yan, J. Wang, Z. Yang, Q. Zhou, H. Luo, S. Qu, Journal of the European Ceramic Society, 40 (2020) 2013-2019.

[4] Z. Cheng, Y. Liu, F. Ye, C. Zhang, H. Qin, J. Wang, L. Cheng, Journal of the European Ceramic Society, 40 (2020) 1149-1158.

[5] M. Zhao, Y. Liu, N. Chai, H. Qin, X. Liu, F. Ye, L. Cheng, L. Zhang, Journal of the European Ceramic Society, 38 (2018) 1334-1340.

[6] R. Mo, X. Yin, F. Ye, X. Liu, X. Ma, Q. Li, L. Zhang, L. Cheng, Journal of the European Ceramic Society, 39 (2019) 743-754.

[7] X. Huang, X. Yan, L. Xia, P. Wang, Q. Wang, X. Zhang, B. Zhong, H. Zhao, G. Wen, Scripta Materialia, 120 (2016) 107-111.

[8] X. Huang, M. Lu, X. Zhang, G. Wen, Y. Zhou, L. Fei, Scripta Materialia, 67 (2012) 613-616.

[9] H. Tian, H.T. Liu, H.F. Cheng, Composites Science and Technology, 90 (2014) 202-208.

[10] H. Luo, Y. Tan, Y. Li, P. Xiao, L. Deng, S. Zeng, G. Zhang, H. Zhang, X. Zhou, S. Peng, Journal of the European Ceramic Society, 37 (2017) 1961-1968.

[11] Y. Qing, Y. Mu, Y. Zhou, F. Luo, D. Zhu, W. Zhou, Journal of the European Ceramic Society, 34 (2014) 2229-2237.

[12] Y. Mu, W. Zhou, Y. Hu, H. Wang, F. Luo, D. Ding, Y. Qing, Journal of the European Ceramic Society, 35 (2015) 2991-3003.

[13] F. Ye, L. Zhang, X. Yin, Y. Zhang, L. Kong, Q. Li, Y. Liu, L. Cheng, Journal of the European Ceramic Society, 33 (2013) 1469-1477.

[14] X. Yuan, L. Cheng, S. Guo, L. Zhang, Ceramics International, 43 (2017) 282-288.

[15] W.L. Song, M.S. Cao, Z.L. Hou, J. Yuan, X.Y. Fang, Scripta Materialia, 61 (2009) 201-204.

[16] F. Wan, F. Luo, H. Wang, Z. Huang, W. Zhou, D. Zhu, Ceramics International, 40 (2014) 15849-15857.

[17] F. Wan, F. Luo, Y. Mu, Z. Zeng, W. Zhou, Ceramics International, 41 (2015) 9957-9965.

[18] F. Wan, F. Luo, Y. Shi, W. Zhou, D. Zhu, International Journal of Applied Ceramic Technology, 12 (2015) 1045-1053.

[19] S. Hoshii, A. Kojima, T. Tamaki, S. Otani, Journal of Materials Science Letters, 19 (2000) 557-560.

[20] H. Schneider, J. Schreuer, B. Hildmann, Journal of the European Ceramic Society, 28

(2008) 329-344.

[21] A. Nicolson, G. Ross, Instrumentation and Measurement, IEEE Transactions on, 19 (1970) 377-382.

[22] J. Baker-Jarvis, E.J. Vanzura, W.A. Kissick, Microwave Theory and Techniques, IEEE Transactions on, 38 (1990) 1096-1103.

[23] W.F. Horn, F.A. Hummel, Journal of the American Ceramic Society, 63 (1980) 338-339.

[24] P. Robinson, E.R. McCartney, Journal of the American Ceramic Society, 47 (1964) 587-592.